energy&fuels

pubs.acs.org/EF

Article

Investigation into the Pyrolysis Bond Dissociation Enthalpies (BDEs) of a Model Lignin Oligomer Using Density Functional Theory (DFT)

Ross W. Houston, Thomas J. Elder, and Nourredine H. Abdoulmoumine*

Cite This: *Energy Fuels* 2022, 36, 1565−1573

Read Online

ACCESS | Metrics & More | Article Recommendations | Supporting Information

ABSTRACT: Pyrolysis is a promising technology for converting lignocellulosic biomass into chemicals, materials, and fuels. Understanding the fundamental reactions and mechanisms during the fast pyrolysis of lignocellulosic biomass is essential for improving the efficiency of this technology. Investigations of lignin fast pyrolysis reactions and mechanisms have thus far lagged relative to cellulose and hemicellulose and have largely been focused on lignin model dimers and monomers. These studies provide valuable information about the reaction tendencies of individual linkages; however, the complex and varying nature of lignin interunit linkages does not allow direct extrapolation to larger lignin structures. In this study, we computationally investigate homolytic bond scission reactions of a larger, synthesizable model lignin oligomer, containing three major lignin linkages, using density functional theory. The bond dissociation enthalpies of the model oligomer showed the trend for the four lowest BDEs C_α−O (β-5) < C_α−C_β (β-5) < C_α−O (α-O-4) < C_β−O (β-O-4). Our results show that the general trends identified in smaller dimer molecules are maintained while the magnitude of the BDEs is increased in the model oligomer. This work is an important first step in developing a library of reaction information for various lignin substructures.

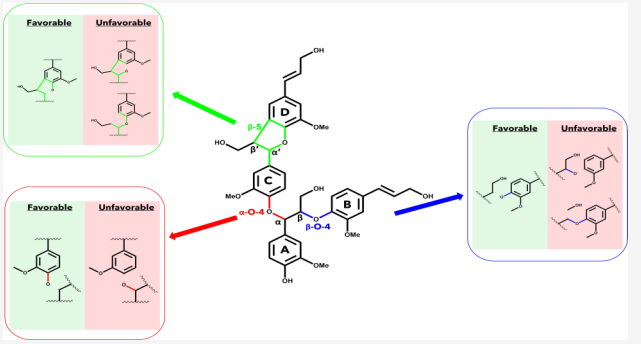

INTRODUCTION

Fast pyrolysis of biomass is a thermochemical process that occurs at low gas residence times (<2 s), high heating rates (200−12 000 °C s^{-1}), and moderate temperatures (400−600 °C) in the absence of oxygen.[1−5] It produces three major products in descending order by yield: solid biochar, light gases, e.g., carbon monoxide, carbon dioxide, hydrogen, and C_1−C_4 hydrocarbons, and bio-oil.[6] Fast pyrolysis has become an attractive technique for converting lignocellulosic biomass because of the promise of bio-oil, which can be upgraded to fuel, chemicals, and products. Throughout the past three decades, there has been a notable increase in attempts to mechanistically understand the transformation of cellulose, hemicellulose, and lignin, the three main constituents of lignocellulosic biomass.[7−12] These efforts are producing the first detailed reaction mechanisms of biomass fast pyrolysis that could be incorporated into reactor models for engineering optimization and scalability investigations.[8,13−17] While these mechanisms are far from perfect, they are nonetheless extremely valuable and provide a starting point for further improvements. The mechanism development studies take different approaches, but all rely on years of both experimental and computational studies on isolated cellulose, hemicellulose, and lignin, as well as model compounds thereof to collate data, propose, and evaluate mechanisms. For example, the cellulose branch of the Ranzi biomass pyrolysis mechanism, one of the leading biomass pyrolysis mechanisms currently, relies on findings on cellulose investigations that go back to the 1970s to propose activated cellulose as the first intermediate and levoglucosan as a major product.[18,19] Historically, cellulose, hemicellulose, and their model compounds have been the subject of more pyrolysis investigations, in part, because they are structurally less complex than lignin.[17,20] However, as fast pyrolysis mechanisms are improved, it is imperative to investigate oligomeric lignin model compounds with different interunit linkages to provide improved mechanistic insights.

Lignin is one of the most abundant biopolymers in the world and constitutes up to 35 wt % of lignocellulosic biomass.[21−23] Lignin provides strength, rigidity, and hydrophobicity to the secondary cell wall of plants.[24] Lignin synthesis is complex and consists of three steps: (1) biosynthesis of monomers, (2) transport, and (3) polymerization.[25] The monolignols are synthesized in the cytosol and then transported to the secondary cell wall.[26,27] There, lignin is synthesized via the radical polymerization of three major hydroxycinnamyl alcohol subunits (*p*-coumaryl, coniferyl, and sinapyl alcohol) by

Received: September 22, 2021
Revised: January 4, 2022
Published: January 14, 2022

https://doi.org/10.1021/acs.energyfuels.1c03238
Energy Fuels 2022, 36, 1565−1573

peroxidase and laccase, which results in lignin being an amorphous, racemic polymer with an aromatic nature.[28] The complexity and lack of a well-defined structure presents challenges when investigating lignin fast pyrolysis, as discussed in the next sections.

Several researchers have investigated model lignin substructures that are representative of what can be found in native lignin.[10,29−36] These model compounds range from the monomeric bases of major pyrolysis products, such as guaiacol and syringol, to model dimers and trimers that contain various critical interunit linkages (β-O-4, α-O-4, β-5, and others) and give rise to the complexity of the lignin structure. Bond dissociation enthalpies (BDEs) and major pyrolysis pathways for these model compounds have been developed through computational and experimental investigation with the hope of better understanding the pyrolysis nature of native lignin.

Until recently, most computational mechanistic studies on lignin model compounds have been limited to monomers, dimers, and trimers, with most focusing on the β-O-4 linkage, which accounts for approximately 60% of all lignin linkages.[17] The kinetics and mechanisms of dimers and trimers, such as phenethyl phenyl ether (PPE),[36−38] offer valuable insights but, because they contain limited interunit linkages, they are not directly applicable to native lignin. Therefore, it is imperative to investigate larger oligomeric substructures that include multiple interunit linkages and are more representative of lignin fractions that are observed during thermal degradation.

The recent advances in computational chemistry and continued improvements in access to and power of high-performance computing infrastructures provide an opportunity to investigate the thermal degradation of model lignin oligomers to gain further mechanistic insight into the pathways involved in native lignin pyrolysis and their associated energetics.[39] Density functional theory (DFT) has been used extensively for simulating the pyrolysis of lignin model compounds due to its increased computational efficiency and comparable accuracy to other ab initio methods, such as Hartree−Fock methods.[40] Additionally, DFT explicitly addresses electron correlation, which otherwise would require more expensive post-Hartree−Fock methods. DFT calculations can identify the location of essential points on the potential energy surface (reactants, products, transition states) that allow for the determination of activation energetics and kinetics associated with specific reactions. Previous computational investigations of model lignin monomers, dimers, and trimers have identified trends between the relative strengths of several homolytic cleavage reactions, with the β-O bond having the lowest BDE. Additionally, DFT calculations have provided insight into the temperature dependence on the dominant reaction type during lignin pyrolysis, free radical, or concerted.[10,41] DFT is already beginning to be used in this matter, with at least two studies that we are aware of exploring the lignin substructures up to decamers in some cases.[27,42,43] Larger oligomeric substructures of lignin allow for simultaneous investigation of the degradation behavior of multiple interunit linkages as well as identification of any potential effects caused by adjacent linkages. The authors of the current work believe that identifying reactivity trends over a variety of linkages can be leveraged to better understand the pyrolysis behavior of native lignin. The development of a mechanistic understanding of lignin's deconstruction during pyrolysis will bring us closer to developing a full mechanistic reaction scheme for whole biomass pyrolysis. The authors believe that a promising way of developing a reaction mechanism that can account for the varying structure of lignin is to systematically investigate a variety of lignin substructures computationally and experimentally, identify reactivity trends, collate findings into a library of lignin reaction information, and postulate reaction rules, hierarchy, and mechanisms that can be applied to different lignin structures. This work is a modest first step toward developing the library of reaction information by computationally investigating the BDEs of free-radical bond scissions using DFT for a chosen model lignin tetramer that contains three important interunit linkages (β-O-4, α-O-4, and β-5) found in native lignin.

MATERIALS AND METHODS

Model Lignin Oligomer. The chosen lignin oligomer, *erythro*-guaiacylglycerol-α-dehydrodiconiferyl-β-coniferyl-bis-ether, is made up of coniferyl units, contain β-O-4, α-O-4, and β-5 linkages, and has been previously synthesized in appreciable yields.[44,45] The model oligomer's structure is shown in Figure 1. The model oligomer was selected to correspond with the experimental literature of synthesizable lignin model compounds. Computational investigation of this oligomer will be compared to the future experimental pyrolysis behavior of the synthesized oligomer. To the best of the authors' knowledge, this work will be the first computational investigation into a model lignin oligomer with three different interunit linkage types, which captures three prevalent linkages found in native lignin.

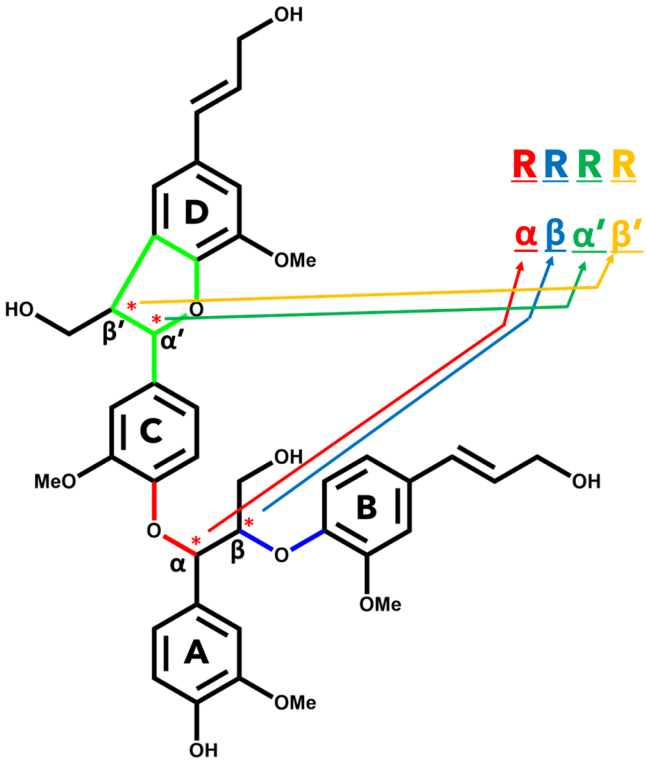

Figure 1. Skeletal structure of the model lignin oligomers. Relevant interunit linkages are highlighted by colors: β-O-4 (blue), α-O-4 (red), and β-5 (green). (*) indicates chiral centers.

The model compound has several noteworthy characteristics. First, there are four chiral centers in this compound, which produce 16 possible stereoisomers that must be appropriately treated in the following sections. In the Results and Discussion section, the investigated stereoisomers are presented using a naming nomenclature introduced in Figure 1. Each chiral center is labeled by its carbon position (α, β, α', and β'), and each position is represented by its

https://doi.org/10.1021/acs.energyfuels.1c03238
Energy Fuels 2022, 36, 1565−1573

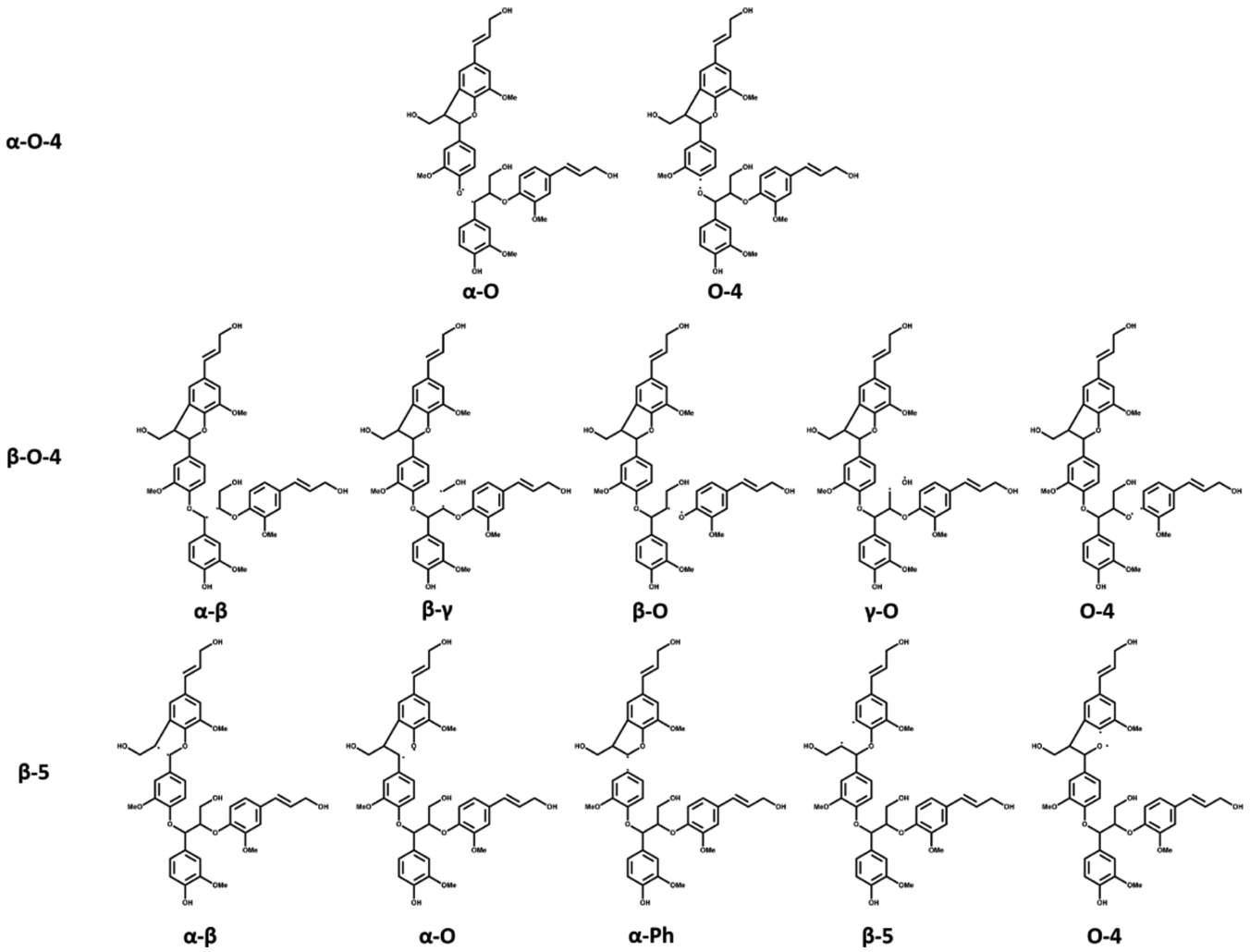

Figure 2. List of homolytic reactions investigated for the model lignin oligomer.

absolute configuration (*R* or *S*), depending on the spatial arrangement of atoms around the respective chiral center. The stereocenter labeling of *R* and *S* is used to differentiate between enantiomers of a chiral compound. The substituents of a chiral center are given priority by their atomic numbers. If the relative priority of the substituents follows a clockwise direction, the chiral center is labeled as *R* configuration. Likewise, if the relative direction is counterclockwise, the chiral center is in the *S* configuration. An example of the naming nomenclature of our model compound is as follows: if both C-α and C-β' are *S* configurations, while the other two are *R*, the resulting designation would be *SRRS*. The other notable characteristic is the presence of a noncyclic α-aryl ether linkage. This type of linkage has been identified in synthetic lignin oligomers; however, there is no experimental data to support the existence of this linkage in native lignin.[28] Even so, this combination of prevalent interunit linkages can provide valuable information on the behavior of this lignin substructure and will allow for the investigation into the effect of adjacent linkages on the bond dissociation enthalpies of specific linkages.

Computational Details. The computational work in this study was done using Spartan '18 (Wavefunction, Inc., Irvine, CA, 2018), GaussView 6, and Gaussian 16 (Gaussian, Inc., Wallingford, CT, 2016). The density functional theory (DFT) calculations were performed on the Infrastructure for Scientific Applications and Advanced Computing (ISAAC) high-performance computing resource at the University of Tennessee and using the resources of the Alabama Supercomputer Authority. The computational setup was divided into two phases that are discussed in the following sections: conformational analysis and determination of bond dissociation enthalpies (BDEs).

Conformational Analysis. Due to the radical polymerization of monomers at the β position during lignin synthesis, lignin oligomers have multiple chiral centers.[28] The stereochemistry of lignin has the potential to play a role in reactivity and product formation.[46] Therefore, we must investigate each possible stereoisomer of the chosen oligomer. Fortunately, it has been reported that the enthalpies calculated via DFT for enantiomers are within "chemical accuracy", so we only need to consider one set of enantiomeric pairs.[42,46,47] Four chiral centers lead to 16 possible stereoisomers consisting of eight enantiomeric pairs. We performed a Monte Carlo conformational analysis of eight stereoisomers in Spartan '18 to identify the lowest energy conformer to use in our DFT calculations. The search identified the 500 lowest energy conformers using the molecular mechanics force field MMFF94[48] and was further filtered down to the 10 lowest energy conformers using a semiempirical PM6 optimization method.[49] The 10 remaining conformers were exported to Gaussian 16 and optimized using the M06-2X hybrid functional and the 6-31+G(d) basis set to identify the lowest energy conformer.[50−53] A geometry optimization and frequency analysis were performed on the lowest energy conformation for each stereoisomer at the M06-2X/6-311++G(d,p) level of theory.[54] The dispersion interactions were described using the GD3 empirical dispersion correction.[55]

After completion of the conformation analysis and optimization, the structure of each stereoisomer was investigated to identify any potential dimeric interactions, such as parallel or T-shaped conformations between the aromatic rings, indicative of π

https://doi.org/10.1021/acs.energyfuels.1c03238
Energy Fuels 2022, 36, 1565−1573

interactions. This analysis was accomplished via determination of the interatomic distances between aromatic rings and the calculation of the ring angles relative to each other. Each aromatic ring was labeled as A–D (Figure 1). The interatomic distances were calculated as the distances between the centroid of the respective ring, and the angles were calculated as the angle between the planes of the respective rings.

Determination of Bond Scission Energetics. The model oligomer's energetics and dissociation products were determined via geometry optimization and frequency analysis at both 298.15 and 773.15 K at the M06-2X/6-311++G(d,p) level of theory. A temperature of 773.15 K is a well-documented and widely used temperature for biomass fast pyrolysis. Simulations at the elevated temperature ensure that the calculated energetics are relevant for the operating conditions of fast pyrolysis. The structure of the radical products was generated from the lowest energy conformer for each stereoisomer. This allows for the preservation of structural components while more accurately modeling the strength of the cleaved bonds.[46] The products of the β-O-4 and α-O-4 scissions consist of two separate, singlet radical species. These species are optimized and analyzed separately. However, for the β-5 ring-opening scissions, the resulting product is a single molecule with two unpaired electrons. Special care was taken to eliminate rebonding during the geometry optimization. The molecules were optimized as triplets and given an initial interatomic distance of 2.5 Å, which has previously been successful for calculating ring-opening reactions.[56] Figure 2 shows the homolytic reactions investigated in this work.

Bond dissociation enthalpies (BDEs) were calculated for the homolytic cleavage of major bonds by calculating the difference between the sum of electronic and thermal enthalpies for the products and the reactants, shown in eq 1

$$\mathrm{BDE} = \sum (e_0 - H_{\mathrm{corr}})_{\mathrm{products}} - \sum (e_0 - H_{\mathrm{corr}})_{\mathrm{reactants}}$$
$$H_{\mathrm{corr}} = E_{\mathrm{tot}} + k_{\mathrm{B}}T \quad (1)$$

where e_0 is the total electronic energy, H_{corr} is the thermal correction to enthalpy, E_{tot} is the total internal energy, and k_{B} is the Boltzmann constant.[57] Bond dissociation enthalpies (BDEs) were determined from calculations at 298.15 and 773.15 K and are referred to as ΔH_{298} and ΔH_{773}, respectively.

RESULTS AND DISCUSSION

Conformational Analysis. The electronic energies of the model tetramer, accounting for thermal correction to enthalpy, for each stereoisomer's 10 lowest energy conformers were calculated at 298.15 K using the M06-2X/6-31+g(d) level of theory. Different configurations had a range of enthalpies of 3.79–16.28 kcal mol^{-1}, depending on the stereoisomer. The resulting lowest energy conformers were then optimized using M06-2X/6-311++G(d,p) to determine the initial tetramer for each stereoisomer, shown in Table 1. The range of enthalpies between stereoisomers was 5.30 kcal mol^{-1}. This range falls outside of the range of ±1.00 kcal mol^{-1} of chemical accuracy, so several of the stereoisomers are appreciably different.[42] *RSSR* and *RRSS* were the least stable isomers with indistinguishable differences in their enthalpies, while *RSSS* and *RSRS* were the most stable stereoisomers and indistinguishable from each other. This range of enthalpies is enough to conclude that stereochemistry can appreciably affect the energetics of a system. With additional investigation, it may provide some insight into the range of possible structures in a native oligomer.

The interatomic distances between aromatic rings were calculated from the centroids of the respective rings, labeled in Figure 3, and the measured ring angles were calculated as the angles formed between the planes of the respective rings. The calculated distances and angles are shown in Tables 2 and 3, respectively. Equilibrium distances for specific conformations

Table 1. Relative Enthalpy Difference of the Optimized Structure for Each Stereoisomer of the Model Tetramer at the M06-2X/6-311++G(d,p) Level of Theory at 298.15 K

configuration	relative enthalpy difference (kcal mol^{-1})
RRRR	1.26
RRRS	3.88
RRSR	4.07
RRSS	0.66
RSRR	3.48
RSRS	4.30
RSSR	0
RSSS	5.30

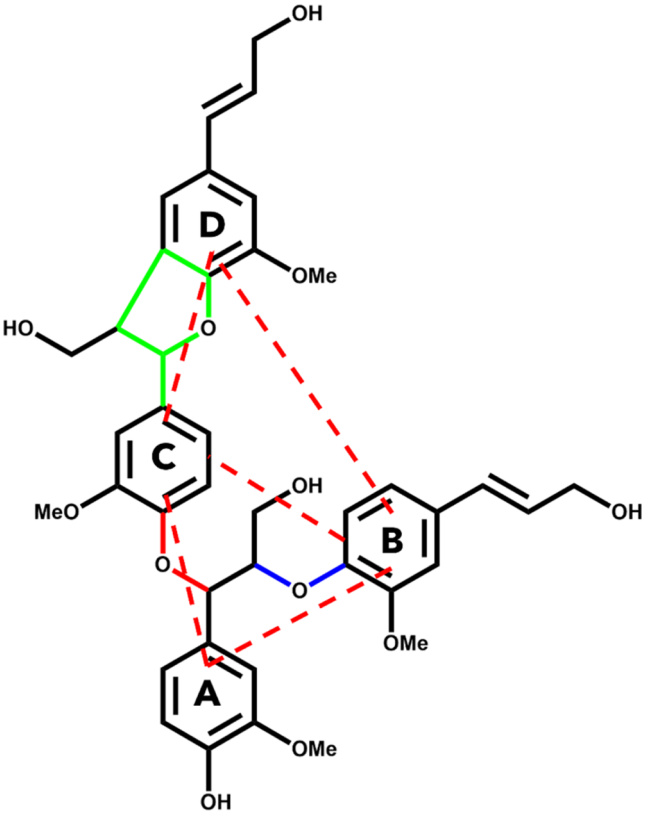

Figure 3. Visualization of interatomic distances and ring angle calculations.

Table 2. Interatomic Distances between Aromatic Rings of Different Stereoisomers of the Model Tetramer

	interatomic distances (Å)					
	A–B	A–C	A–D	B–C	B–D	C–D
RRRR	6.51	6.30	10.92	4.79	6.38	5.50
RRRS	6.66	6.29	11.57	4.18	6.33	5.89
RRSR	6.72	6.30	11.50	3.89	5.40	5.90
RRSS	6.55	6.04	10.77	5.16	6.23	5.27
RSRR	7.16	6.26	9.83	5.00	5.26	5.01
RSRS	6.67	6.34	10.99	4.16	5.38	5.39
RSSR	6.41	5.63	10.77	4.01	6.43	5.19
RSSS	6.68	5.33	10.54	4.05	7.21	5.30

https://doi.org/10.1021/acs.energyfuels.1c03238
Energy Fuels 2022, 36, 1565–1573

Table 3. Ring Angles between the Aromatic Rings of Different Stereoisomers of the Model Tetramer

	ring angle (deg)					
	A−B	A−C	A−D	B−C	B−D	C−D
RRRR	61.77	59.42	89.66	25.29	49.36	74.05
RRRS	60.67	49.99	76.91	16.88	54.95	71.82
RRSR	55.61	53.86	80.57	3.09	45.78	48.80
RRSS	57.37	68.58	36.23	30.94	59.14	85.71
RSRR	63.10	33.63	82.49	64.00	31.67	85.88
RSRS	36.64	48.45	80.29	12.07	74.86	77.12
RSSR	54.15	78.80	14.16	30.41	64.77	85.22
RSSS	68.01	88.00	7.19	20.78	61.86	82.20

have been previously calculated by Tsuzuki et al.[58] Parallel configurations of aromatic rings had an equilibrium interatomic distance of approximately 3.80−4.00 Å. Additionally, the planes of the aromatic rings do not intersect in a parallel configuration. The other major configuration type is T-shaped or edge-to-face with equilibrium distances of 5.00−5.20 Å and perpendicular ring angles.[58]

As evidenced by the values in Tables 2 and 3, the most likely candidates for parallel or T-shaped configurations are the B−C rings, which correspond to the aromatic rings at the end of the β-O-4 and α-O-4 linkages. As the interatomic distances between B−C approach the previously mentioned equilibrium distances, we would expect an increased π/π interaction, which could give rise to increased stability of a specific stereoisomer. For example, the *RRSR* stereoisomer has a B−C interatomic distance of 3.89 Å and an almost parallel angle (3.09°), suggesting a potential parallel configuration, which could explain the increase in stability of the *RRSR* compared to the least stable isomers of *RSSR* and *RRSS*. The optimized geometry of each stereoisomer is shown in Figure 4, and three-dimensional Cartesian coordinates of these stereoisomers are shown in the Supporting Information.

Bond Dissociation Enthalpies (BDEs). The bond dissociation enthalpies were initially calculated for each relevant bond in the three interunit linkages found in the tetramer. The nomenclature for the reactions discussed in this section is based on the α and β positions of the relevant chiral carbons. The homolytic reactions investigated are shown in Figure 2. Upon convergence, the optimized geometries were subjected to a vibrational frequency analysis at 298.15 and 773.15 K to calculate the BDEs for room temperature and a relevant pyrolysis temperature. The BDEs for both temperatures can be seen in Tables 4 and 5, respectively.

Upon comparison of the BDE calculations, several trends were identified. The magnitude of ΔH_{298} values is slightly different from that of ΔH_{773}, which is to be expected. However, the overall trends present at 298.15 K remain at a pyrolysis reaction temperature of 773.15 K. Overall, the carbon−oxygen bonds for a specific linkage are shown to be easier to break than the carbon−carbon bonds. The β-O and the α-O bonds in the ether linkages had ΔH_{773} with a range of 74.67−86.78 and 61.88−76.10 kcal mol^{-1}, respectively. Both the trend and overall magnitudes of these BDEs were expected and agreed with previous BDE investigations.[59,60] The aromatic carbon−oxygen bonds in the ether linkages, e.g., O-4 bond in a β-O-4 linkage, are the exception as they are harder to break than their nonaromatic counterparts (111.16−121.37 kcal mol^{-1}), which also agrees with the findings from Huang et al.[41] The same general trend of C−O having a lower BDE than that of C−C can be seen in the C_α−O and C_α−C_β bonds for the β-5 ring-opening scission reactions, which are significantly easier to break than the aromatic C−O and C−C bonds. The C_α−O bond had a 46.25−55.75 kcal mol^{-1} range, and the C_α−C_β bond ranged from 57.76 to 71.49 kcal mol^{-1}, while the aromatic bonds had a much higher BDE of 86.06−118.13 kcal mol^{-1}. The lower BDE of the nonaromatic bonds can be attributed to the delocalization of electrons along the aromatic ring. Additionally, homolytic cleavage involving an aromatic ring would result in a radical on the carbon ring, which would disrupt the aromaticity. This trend was also reported by another BDE investigation of dimeric phenylcoumaran substructures.[61] The observed trend for the four lowest BDE scissions at both 298.15 and 773.15 K is C_α−O (β-5) < C_α−C_β (β-5) < C_α−O (α-O-4) < C_β−O (β-O-4). While the trends were consistent, the magnitude of BDEs for individual bonds in the model tetramer was larger than their respective bonds in smaller, dimeric compounds. The BDEs for the β-O bond of substituted β-O-4 dimers were calculated in the range of 68−71 kcal mol^{-1}, which is noticeably lower than the BDEs for the model tetramer.[61] The BDE for the α-O bond of the α-O-4 linkage is similarly larger than that for the corresponding bond (42.4 kcal mol^{-1}) in the α-O-4 dimer studied by Huang and He.[62] The BDEs for the β-5 ring-opening reactions are closer to their dimer counterparts; however, they are still slightly larger than the BDEs calculated for smaller molecules.[10]

Inspection of the spin density plots of the resulting radicals visualizes the delocalization of the unpaired electron around the molecule. The aromatic C-containing bonds exhibit a concentration of the spin density around the radical, whereas the products resulting from nonaromatic C−O bonds have a degree of delocalization of spin density around the neighboring aromatic ring. These observations agree with the trend of BDEs calculated as delocalization is expected to lower the BDE compared to a confined spin density. Spin density plots are reported in the Supporting Information.

It was observed that the least stable stereoisomer, RSSR, from the conformational analysis was regularly on the lower end of the range of BDEs for each reaction. However, this trend did not always hold for the other indistinguishable lower-stability stereoisomer, *RRSS*. This discrepancy can be partially attributed to an inherent error of 1.30 kcal mol^{-1} associated with M06-2X calculations.[63] Additionally, it can be assumed that the stability trends for each conformation of the initial oligomer are not directly transferred to the resulting BDEs for individual reactions for a respective stereoisomer. The adjacent configuration may interact differently on the resulting radical fragments.

This work represents an initial step toward investigating larger, more representative substructures of native lignin. Moving forward, further investigation into this model compound and other oligomers will provide valuable information and bring the community closer to gaining a mechanistic understanding of the deconstruction pathways of native lignin. The valuable mechanistic information gained from these larger structures will improve our knowledge of lignin pyrolysis closer to that of cellulose and hemicellulose.

CONCLUSIONS

The mechanistic understanding of lignin pyrolysis pathways is underdeveloped compared to both cellulose and hemicellulose. To narrow the gap, model lignin compounds have been studied to understand the pyrolysis of simpler lignin structures.

https://doi.org/10.1021/acs.energyfuels.1c03238
Energy Fuels 2022, 36, 1565−1573

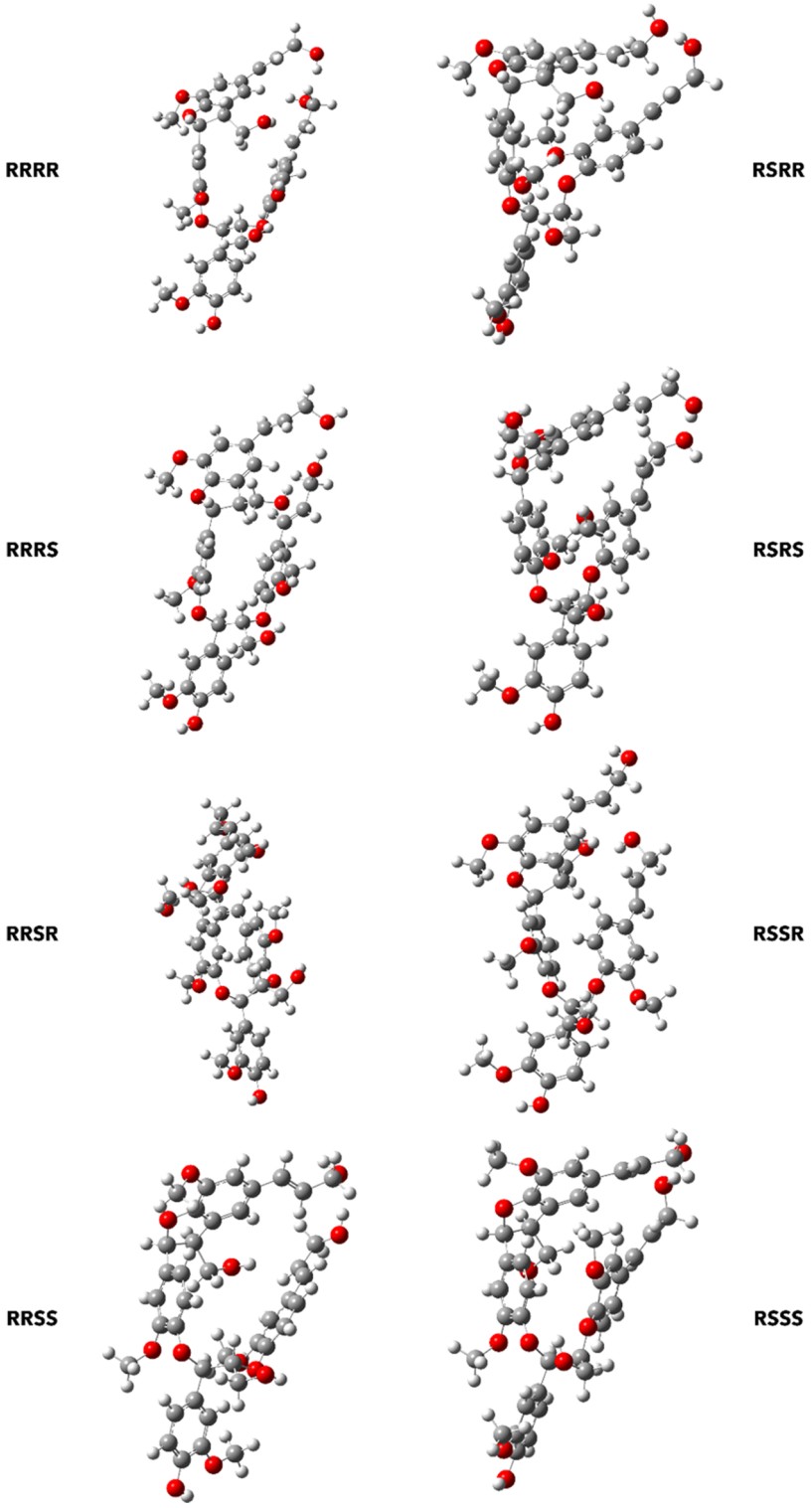

Figure 4. Optimized geometries for each stereoisomer of the model tetramer at M06-2X/6-311++G(d,p).

In this work, the thermal behavior of a model lignin oligomer was investigated via density functional theory to determine the energetics associated with homolytic bond cleavage during biomass fast pyrolysis. The chiral complexity of the oligomer required the consideration of multiple stereoisomers, which were found to have a range of enthalpy of 5.30 kcal mol^{-1}. The BDEs (ΔH_{298} and ΔH_{773}) followed the same trend in terms of the relative bond strength, as seen in smaller model lignin molecules. The overall trend observed for the major bond scission was C_α−O (β-5) < C_α−C_β (β-5) < C_α−O (α-O-4) < C_β−O (β-O-4). The nonaromatic C−O bonds were shown to be the easiest to break in all three interunit linkages, which agrees with the previous literature. The homolytic cleavages involving aromatic rings exhibited much higher BDEs due to the stability resulting from electron delocalization and disruption of aromaticity in the resulting products, which was confirmed when visualizing the spin density. This work provides an important first step in developing a library of

https://doi.org/10.1021/acs.energyfuels.1c03238
Energy Fuels 2022, 36, 1565−1573

Table 4. Bond Dissociation Enthalpies, ΔH_{298} (kcal mol^{-1}), for Each Stereoisomer Conformation at 298.15 K

Family	Bond	RRRR	RRRS	RRSR	RRSS	RSRR	RSRS	RSSR	RSSS
α-O-4	α-O	66.88	71.05	72.94	68.10	76.36	70.21	62.18	72.48
	O-4	113.18	117.72	119.58	112.73	119.06	116.29	110.64	117.50
β-O-4	1-α	104.88	101.62	100.26	105.20	106.45	101.00	102.96	111.47
	α-β	90.71	94.00	93.13	92.90	93.17	93.76	91.36	97.37
	β-O	78.14	84.33	81.40	77.77	79.07	77.72	74.70	86.74
	β-γ	88.65	89.58	87.83	91.47	91.96	86.26	87.00	88.36
	γ-O	100.03	103.22	96.45	97.48	96.91	96.06	96.39	96.88
	O-4	114.80	120.44	118.92	116.47	117.47	112.73	111.60	121.67
β-5	α-Ph	113.46	116.03	111.89	109.36	118.24	113.41	108.71	116.14
	β-5	100.00	99.18	96.29	95.05	97.52	98.82	93.81	101.22
	α-O	51.68	51.77	46.20	45.00	54.41	47.64	45.72	53.60
	α-β	66.66	64.17	64.77	65.34	67.55	69.96	69.11	56.97
	O-4	85.18	89.01	93.24	88.64	93.16	94.53	91.79	93.93

Table 5. Bond Dissociation Enthalpies, ΔH_{773} (kcal mol^{-1}), for Each Stereoisomer Conformation at 773.15 K

Family	Bond	RRRR	RRRS	RRSR	RRSS	RSRR	RSRS	RSSR	RSSS
α-O-4	α-O	66.68	70.89	72.80	67.96	76.10	69.92	61.88	72.27
	O-4	112.83	117.48	119.31	112.45	118.66	115.89	110.42	117.00
β-O-4	1-α	104.50	101.23	99.87	104.83	106.18	100.49	102.68	110.97
	α-β	90.86	94.23	93.32	93.27	93.33	93.96	90.70	97.49
	β-O	78.12	84.42	81.34	77.81	78.97	77.67	74.67	86.78
	β-γ	89.01	89.72	88.02	91.81	92.23	86.37	87.27	88.48
	γ-O	101.10	104.44	97.46	98.50	98.06	97.08	97.43	97.87
	O-4	114.22	120.13	118.57	116.22	116.99	112.20	111.16	121.37
β-5	α-Ph	113.27	115.89	111.64	109.21	118.13	113.15	108.46	115.88
	β-5	101.26	100.44	97.47	96.33	98.83	100.12	95.00	102.38
	α-O	52.79	52.96	47.25	46.25	55.75	48.70	47.01	54.70
	α-β	68.48	65.56	66.43	66.95	69.18	71.49	70.65	57.76
	O-4	86.06	90.01	94.00	89.69	94.04	95.40	92.70	94.83

reaction information for various lignin substructures that can be developed into generalized reaction rules for native lignin pyrolysis.

■ ASSOCIATED CONTENT

Supporting Information

The Supporting Information is available free of charge at https://pubs.acs.org/doi/10.1021/acs.energyfuels.1c03238.

Cartesian coordinates for optimized structures and spin density plots for the products for the *RSRS* stereoisomer (PDF)

■ AUTHOR INFORMATION

Corresponding Author

Nourredine H. Abdoulmoumine − *Department of Biosystems Engineering and Soil Science, University of Tennessee, Knoxville, Tennessee 37996, United States; Center for Renewable Carbon, University of Tennessee, Knoxville, Tennessee 37996, United States;* orcid.org/0000-0001-6586-5919; Email: nabdoulm@utk.edu

Authors

Ross W. Houston − *Department of Biosystems Engineering and Soil Science, University of Tennessee, Knoxville, Tennessee 37996, United States;* orcid.org/0000-0002-6505-9535

Thomas J. Elder − *USDA-Forest Service, Auburn, Alabama 36849, United States;* orcid.org/0000-0003-3909-2152

Complete contact information is available at: https://pubs.acs.org/10.1021/acs.energyfuels.1c03238

Notes

The authors declare no competing financial interest.

■ ACKNOWLEDGMENTS

A portion of the computation for this work was performed on the computational resources at the Infrastructure for Scientific Applications and Advanced Computing (ISAAC) supported by the University of Tennessee. Additionally, this work was made possible, in part, by a grant of high-performance computing resources and technical support from the Alabama Supercomputer Authority. This research was supported, in part, by the U.S. Department of Agriculture, U.S. Forest Service.

■ REFERENCES

(1) Maduskar, S.; Facas, G. G.; Papageorgiou, C.; Williams, C. L.; Dauenhauer, P. J. Five Rules for Measuring Biomass Pyrolysis Rates: Pulse-Heated Analysis of Solid Reaction Kinetics of Lignocellulosic Biomass. *ACS Sustainable Chem. Eng.* **2018**, *6*, 1387−1399.

(2) Pecha, M. B.; Montoya, J. I.; Ivory, C.; Chejne, F.; Garcia-Perez, M. Modified Pyroprobe Captive Sample Reactor: Characterization of Reactor and Cellulose Pyrolysis at Vacuum and Atmospheric Pressures. *Ind. Eng. Chem. Res.* **2017**, *56*, 5185−5200.

(3) Hoekstra, E.; van Swaaij, W. P. M.; Kersten, S. R. A.; Hogendoorn, K. J. A. Fast Pyrolysis in a Novel Wire-Mesh Reactor: Design and Initial Results. *Chem. Eng. J.* **2012**, *191*, 45−58.
(4) Dickerson, T.; Soria, J. Catalytic Fast Pyrolysis: A Review. *Energies* **2013**, *6*, 514−538.
(5) Balat, M.; Balat, M.; Kırtay, E.; Balat, H. Main Routes for the Thermo-Conversion of Biomass into Fuels and Chemicals. Part 1: Pyrolysis Systems. *Energy Convers. Manage.* **2009**, *50*, 3147−3157.
(6) Bridgwater, A. V.; Meier, D.; Radlein, D. An Overview of Fast Pyrolysis of Biomass. *Org. Geochem.* **1999**, *30*, 1479−1493.
(7) Mayes, H. B.; Broadbelt, L. J. Unraveling the Reactions That Unravel Cellulose. *J. Phys. Chem. A* **2012**, *116*, 7098−7106.
(8) Zhou, X.; Li, W.; Mabon, R.; Broadbelt, L. J. A Mechanistic Model of Fast Pyrolysis of Hemicellulose. *Energy Environ. Sci.* **2018**, *11*, 1240−1260.
(9) Zhou, X.; Nolte, M. W.; Mayes, H. B.; Shanks, B. H.; Broadbelt, L. J. Experimental and Mechanistic Modeling of Fast Pyrolysis of Neat Glucose-Based Carbohydrates. 1. Experiments and Development of a Detailed Mechanistic Model. *Ind. Eng. Chem. Res.* **2014**, *53*, 13274−13289.
(10) Elder, T.; Beste, A. Density Functional Theory Study of the Concerted Pyrolysis Mechanism for Lignin Models. *Energy Fuels* **2014**, *28*, 5229−5235.
(11) Hosoya, T.; Sakaki, S. Levoglucosan Formation from Crystalline Cellulose: Importance of a Hydrogen Bonding Network in the Reaction. *ChemSusChem* **2013**, *6*, 2356−2368.
(12) Faravelli, T.; Frassoldati, A.; Migliavacca, G.; Ranzi, E. Detailed Kinetic Modeling of the Thermal Degradation of Lignins. *Biomass Bioenergy* **2010**, *34*, 290−301.
(13) Debiagi, P.; Gentile, G.; Cuoci, A.; Frassoldati, A.; Ranzi, E.; Faravelli, T. A Predictive Model of Biochar Formation and Characterization. *J. Anal. Appl. Pyrolysis* **2018**, *134*, 326−335.
(14) Ranzi, E.; Debiagi, P. E. A.; Frassoldati, A. Mathematical Modeling of Fast Biomass Pyrolysis and Bio-Oil Formation. Note I: Kinetic Mechanism of Biomass Pyrolysis. *ACS Sustainable Chem. Eng.* **2017**, *5*, 2867−2881.
(15) Vinu, R.; Broadbelt, L. J. A Mechanistic Model of Fast Pyrolysis of Glucose-Based Carbohydrates to Predict Bio-Oil Composition. *Energy Environ. Sci.* **2012**, *5*, 9808−9826.
(16) Klein, M. T.; Virk, P. S. Modeling of Lignin Thermolysis. *Energy Fuels* **2008**, *22*, 2175−2182.
(17) Hough, B. R.; Schwartz, D. T.; Pfaendtner, J. Detailed Kinetic Modeling of Lignin Pyrolysis for Process Optimization. *Ind. Eng. Chem. Res.* **2016**, *55*, 9147−9153.
(18) Bradbury, A. G. W.; Sakai, Y.; Shafizadeh, F. A Kinetic Model for Pyrolysis of Cellulose. *J. Appl. Polym. Sci.* **1979**, *23*, 3271−3280.
(19) Molton, P. M.; Demmitt, T. F. *Reaction Mechanisms in Cellulose Pyrolysis: A Literature Review*; BNWL-2297 Dep. NTIS, PC A05/MF A01; Battelle Pacific Northwest Labs.: Richland, WA, 1977.
(20) Chu, S.; Subrahmanyam, A. V.; Huber, G. W. The Pyrolysis Chemistry of a β-O-4 Type Oligomeric Lignin Model Compound. *Green Chem.* **2013**, *15*, 125−136.
(21) Patwardhan, P. R.; Brown, R. C.; Shanks, B. H. Understanding the Fast Pyrolysis of Lignin. *ChemSusChem* **2011**, *4*, 1629−1636.
(22) Glasser, W. G. About Making Lignin Great Again—Some Lessons from the Past. *Front. Chem.* **2019**, *7*, No. 565.
(23) Kawamoto, H. Lignin Pyrolysis Reactions. *J. Wood Sci.* **2017**, *63*, 117−132.
(24) Bonawitz, N. D.; Chapple, C. The Genetics of Lignin Biosynthesis: Connecting Genotype to Phenotype. *Annu. Rev. Genet.* **2010**, *44*, 337−363.
(25) Liu, Q.; Luo, L.; Zheng, L. Lignins: Biosynthesis and Biological Functions in Plants. *Int. J. Mol. Sci.* **2018**, *19*, No. 335.
(26) Miao, Y.-C.; Liu, C.-J. Atp-Binding Cassette-Like Transporters Are Involved in the Transport of Lignin Precursors across Plasma and Vacuolar Membranes. *Proc. Natl. Acad. Sci. U.S.A.* **2010**, *107*, 22728−22733.
(27) Azad, T.; Schuler, J. D.; Auad, M. L.; Elder, T.; Adamczyk, A. J. Model Lignin Oligomer Pyrolysis: Coupled Conformational and Thermodynamic Analysis of β-O-4′ Bond Cleavage. *Energy Fuels* **2020**, *34*, 9709−9724.
(28) Ralph, J.; Lapierre, C.; Boerjan, W. Lignin Structure and Its Engineering. *Curr. Opin. Biotechnol.* **2019**, *56*, 240−249.
(29) Zhu, X.; Lobban, L. L.; Mallinson, R. G.; Resasco, D. E. Bifunctional Transalkylation and Hydrodeoxygenation of Anisole over a Pt/Hbeta Catalyst. *J. Catal.* **2011**, *281*, 21−29.
(30) Huang, X.; Liu, C.; Huang, J.; Li, H. Theory Studies on Pyrolysis Mechanism of Phenethyl Phenyl Ether. *Comput. Theor. Chem.* **2011**, *976*, 51−59.
(31) Huang, J.-b.; Wu, S.-b.; Cheng, H.; Lei, M.; Liang, J.-j.; Tong, H. Theoretical Study of Bond Dissociation Energies for Lignin Model Compounds. *J. Fuel Chem. Technol.* **2015**, *43*, 429−436.
(32) Huang, J.-b.; Liu, C.; Ren, L.-r.; Tong, H.; Li, W.-m.; Wu, D. Studies on Pyrolysis Mechanism of Syringol as Lignin Model Compound by Quantum Chemistry. *J. Fuel Chem. Technol.* **2013**, *41*, 657−666.
(33) Huang, J.; Li, X.; Wu, D.; Tong, H.; Li, W. Theoretical Studies on Pyrolysis Mechanism of Guaiacol as Lignin Model Compound. *J. Renewable Sustainable Energy* **2013**, *5*, No. 043112.
(34) Elder, T. A Computational Study of Pyrolysis Reactions of Lignin Model Compounds. *Holzforschung* **2010**, *64*, 435−440.
(35) Beste, A.; Buchanan, A. C. Computational Study of Bond Dissociation Enthalpies for Lignin Model Compounds. Substituent Effects in Phenethyl Phenyl Ethers. *J. Org. Chem.* **2009**, *74*, 2837−2841.
(36) Beste, A.; Buchanan, A. C. Kinetic Simulation of the Thermal Degradation of Phenethyl Phenyl Ether, a Model Compound for the β-O-4 Linkage in Lignin. *Chem. Phys. Lett.* **2012**, *550*, 19−24.
(37) Beste, A.; Buchanan, A. C. Kinetic Analysis of the Phenyl-Shift Reaction in B-O-4 Lignin Model Compounds: A Computational Study. *J. Org. Chem.* **2011**, *76*, 2195−2203.
(38) Klein, M. T.; Virk, P. S. Model Pathways in Lignin Thermolysis. 1. Phenethyl Phenyl Ether. *Ind. Eng. Chem. Fundam.* **1983**, *22*, 35−45.
(39) Sangha, A. K.; Petridis, L.; Smith, J. C.; Ziebell, A.; Parks, J. M. Molecular Simulation as a Tool for Studying Lignin. *Environ. Prog. Sustainable Energy* **2012**, *31*, 47−54.
(40) Tanaka, A.; Maekawa, K.; Suzuki, K. *Theoretical Calculations in Reaction Mechanism Studies*; R&D Report for Sumitomo Chemical Co., Ltd., 2013; pp 1−10.
(41) Huang, J.; Liu, C.; Wu, D.; Tong, H.; Ren, L. Density Functional Theory Studies on Pyrolysis Mechanism of β-O-4 Type Lignin Dimer Model Compound. *J. Anal. Appl. Pyrolysis* **2014**, *109*, 98−108.
(42) Elder, T.; Berstis, L.; Beckham, G. T.; Crowley, M. F. Density Functional Theory Study of Spirodienone Stereoisomers in Lignin. *ACS Sustainable Chem. Eng.* **2017**, *5*, 7188−7194.
(43) Azad, T.; Torres, H. F.; Auad, M. L.; Elder, T.; Adamczyk, A. J. Isolating Key Reaction Energetics and Thermodynamic Properties During Hardwood Model Lignin Pyrolysis. *Phys. Chem. Chem. Phys.* **2021**, *23*, 20919−20935.
(44) Quideau, S.; Ralph, J. A Biomimetic Route to Lignin Model Compounds Via Silver (I) Oxide Oxidation. 1. Synthesis of Dilignols and Non-Cyclic Benzyl Aryl Ethers. *Holzforschung* **1994**, *48*, 12−22.
(45) Freudenberg, K.; Friedmann, M. Oligomere Zwischenprodukte Der Ligninbildung. *Chem. Ber.* **1960**, *93*, 2138−2148.
(46) Berstis, L.; Elder, T.; Crowley, M.; Beckham, G. T. Radical Nature of C-Lignin. *ACS Sustainable Chem. Eng.* **2016**, *4*, 5327−5335.
(47) Elder, T.; Berstis, L.; Beckham, G. T.; Crowley, M. F. Coupling and Reactions of 5-Hydroxyconiferyl Alcohol in Lignin Formation. *J. Agric. Food Chem.* **2016**, *64*, 4742−4750.
(48) Halgren, T. A. Merck Molecular Force Field. I. Basis, Form, Scope, Parameterization, and Performance of Mmff94. *J. Comput. Chem.* **1996**, *17*, 490−519.
(49) Stewart, J. J. P. Optimization of Parameters for Semiempirical Methods V: Modification of Nddo Approximations and Application to 70 Elements. *J. Mol. Model.* **2007**, *13*, 1173−1213.
(50) Zhao, Y.; Truhlar, D. G. The M06 Suite of Density Functionals for Main Group Thermochemistry, Thermochemical Kinetics,

https://doi.org/10.1021/acs.energyfuels.1c03238
Energy Fuels 2022, 36, 1565−1573

Noncovalent Interactions, Excited States, and Transition Elements: Two New Functionals and Systematic Testing of Four M06-Class Functionals and 12 Other Functionals. *Theor. Chem. Acc.* **2008**, *120*, 215−241.
(51) Hehre, W. J.; Ditchfield, R.; Pople, J. A. Self—Consistent Molecular Orbital Methods. Xii. Further Extensions of Gaussian—Type Basis Sets for Use in Molecular Orbital Studies of Organic Molecules. *J. Chem. Phys.* **1972**, *56*, 2257−2261.
(52) Hariharan, P. C.; Pople, J. A. The Influence of Polarization Functions on Molecular Orbital Hydrogenation Energies. *Theor. Chim. Acta* **1973**, *28*, 213−222.
(53) Clark, T.; Chandrasekhar, J.; Spitznagel, G. W.; Schleyer, P. V. R. Efficient Diffuse Function-Augmented Basis Sets for Anion Calculations. Iii. The 3-21+G Basis Set for First-Row Elements, Li−F. *J. Comput. Chem.* **1983**, *4*, 294−301.
(54) Krishnan, R.; Binkley, J. S.; Seeger, R.; Pople, J. A. Self-Consistent Molecular Orbital Methods. Xx. A Basis Set for Correlated Wave Functions. *J. Chem. Phys.* **1980**, *72*, 650−654.
(55) Grimme, S.; Antony, J.; Ehrlich, S.; Krieg, H. A Consistent and Accurate Ab Initio Parametrization of Density Functional Dispersion Correction (Dft-D) for the 94 Elements H-Pu. *J. Chem. Phys.* **2010**, *132*, No. 154104.
(56) Elder, T. Bond Dissociation Enthalpies of a Dibenzodioxocin Lignin Model Compound. *Energy Fuels* **2013**, *27*, 4785−4790.
(57) Ochterski, J. W. *Thermochemistry in Gaussian*; Gaussian, Inc., 2000; Vol. *1*, p 19.
(58) Tsuzuki, S.; Honda, K.; Uchimaru, T.; Mikami, M.; Tanabe, K. Origin of Attraction and Directionality of the Π/Π Interaction: Model Chemistry Calculations of Benzene Dimer Interaction. *J. Am. Chem. Soc.* **2002**, *124*, 104−112.
(59) Kim, S.; Chmely, S. C.; Nimlos, M. R.; Bomble, Y. J.; Foust, T. D.; Paton, R. S.; Beckham, G. T. Computational Study of Bond Dissociation Enthalpies for a Large Range of Native and Modified Lignins. *J. Phys. Chem. Lett.* **2011**, *2*, 2846−2852.
(60) Parthasarathi, R.; Romero, R. A.; Redondo, A.; Gnanakaran, S. Theoretical Study of the Remarkably Diverse Linkages in Lignin. *J. Phys. Chem. Lett.* **2011**, *2*, 2660−2666.
(61) Younker, J. M.; Beste, A.; Buchanan, A. C. Computational Study of Bond Dissociation Enthalpies for Lignin Model Compounds: *β*-5 Arylcoumaran. *Chem. Phys. Lett.* **2012**, *545*, 100−106.
(62) Huang, J.; He, C. Pyrolysis mechanism of *α*-O-4 linkage lignin dimer: A theoretical study. *J. Anal. Appl. Pyrolysis* **2015**, *113*, 655−664.
(63) Zhao, Y.; Truhlar, D. G. Density Functionals with Broad Applicability in Chemistry. *Acc. Chem. Res.* **2008**, *41*, 157−167.

https://doi.org/10.1021/acs.energyfuels.1c03238
Energy Fuels 2022, 36, 1565−1573